NASA/TM–20250006515

A Summary of Results from Phase 2 Dynamic Drop Testing of Energy Storage Systems for electric Vertical Take-off and Landing (eVTOL) Vehicles

Justin D. Littell, Nathaniel W. Gardner, Matlock M. Mennu

Langley Research Center, Hampton, Virginia

July 2025

NASA STI Program Report Series

Since its founding, NASA has been dedicated to the advancement of aeronautics and space science. The NASA scientific and technical information (STI) program plays a key part in helping NASA maintain this important role.

The NASA STI program operates under the auspices of the Agency Chief Information Officer. It collects, organizes, provides for archiving, and disseminates NASA's STI. The NASA STI program provides access to the NTRS Registered and its public interface, the NASA Technical Reports Server, thus providing one of the largest collections of aeronautical and space science STI in the world. Results are published in both non-NASA channels and by NASA in the NASA STI Report Series, which includes the following report types:

- TECHNICAL PUBLICATION. Reports of completed research or a major significant phase of research that present the results of NASA Programs and include extensive data or theoretical analysis. Includes compilations of significant scientific and technical data and information deemed to be of continuing reference value. NASA counterpart of peer-reviewed formal professional papers but has less stringent limitations on manuscript length and extent of graphic presentations.

- TECHNICAL MEMORANDUM. Scientific and technical findings that are preliminary or of specialized interest, e.g., quick release reports, working papers, and bibliographies that contain minimal annotation. Does not contain extensive analysis.

- CONTRACTOR REPORT. Scientific and technical findings by NASA-sponsored contractors and grantees.

- CONFERENCE PUBLICATION. Collected papers from scientific and technical conferences, symposia, seminars, or other meetings sponsored or co-sponsored by NASA.

- SPECIAL PUBLICATION. Scientific, technical, or historical information from NASA programs, projects, and missions, often concerned with subjects having substantial public interest.

- TECHNICAL TRANSLATION. English-language translations of foreign scientific and technical material pertinent to NASA's mission.

Specialized services also include organizing and publishing research results, distributing specialized research announcements and feeds, providing information desk and personal search support, and enabling data exchange services.

For more information about the NASA STI program, see the following:

- Access the NASA STI program home page at http://www.sti.nasa.gov

- Help desk contact information:

https://www.sti.nasa.gov/sti-contact-form/
and select the "General" help request type.

NASA/TM–20250006515

A Summary of Results from Phase 2 Dynamic Drop Testing of Energy Storage Systems for electric Vertical Take-off and Landing (eVTOL) Vehicles

Justin D. Littell, Nathaniel W. Gardner, Matlock M. Mennu

Langley Research Center, Hampton, Virginia

National Aeronautics and
Space Administration

Langley Research Center
Hampton, Virginia 23681-2199

July 2025

The use of trademarks or names of manufacturers in this report is for accurate reporting and does not constitute an official endorsement, either expressed or implied, of such products or manufacturers by the National Aeronautics and Space Administration.

Available from:

NASA STI Program / Mail Stop 050
NASA Langley Research Center
Hampton, VA 23681-2199

Introduction

Advanced Air Mobility (AAM) vehicles will soon be joining the fleets of current aircraft and rotorcraft as new forms of transportation within airspaces around the world. These new types of vehicles have features that are unlike current fleets, which often contain new materials and manufacturing methods and are designed with non-traditional propulsion systems. These new aircraft are designed to be capable of providing services for a variety of uncrewed missions including package delivery, medical transport, disaster relief and firefighting, as well as passenger carrying missions such as air taxi. The business use case for these types of aircraft requires frequent operation with high utilization rates, operations in the urban environment, and for taxi carrying services, price-points comparable to traditional methods of transportation currently available for use. The market is poised to begin test flights with a handful of vehicles currently undergoing flight testing, making this changing landscape closer to reality.

Due to the unique nature of these vehicles, operational regimes, and propulsion systems, certification efforts are ongoing, and the methods for their certification are active areas of study in government regulatory bodies, industry, and researchers. Regulations covering various aspects related to the aircraft including structures, flight controls, equipment and powerplant are necessary. For the powerplant, and specifically the Energy Storage Systems (ESS) as they relate to the electric engine(s), the requirements for certification involving crash and impact scenarios are currently under development.

In the United States, there are two examples in the Federal Register [1][2] which discuss specifics for certification guidelines under the 14 CFR § 21.17(b) which covers special classes of aircraft. In addressing comments pertaining to the development of crashworthiness requirements for ESS, for example using ref 2, the FAA states "*risks identified are adequately addressed by the requirements of Subparts E and F, AM1.1529 and Appendix A ICA* (which are already proposed requirements) *for airframe, engines, and propellers, with specific safety objectives*" and that specific Means of Compliance (MoC) will be developed for each aircraft "*with specific safety objectives and means of compliance to address these risks that will be developed and tailored to the specific aspects of the [aircraft].*" Future certification efforts may still utilize the "special classes of aircraft" designation or there may be eventual specific regulatory text written that pertains specifically to the crashworthiness of ESS used as primary means of propulsion for specific classes and/or types of vehicles. In either respect, a MoC will be required.

The European Union Aviation Safety Agency (EASA) has accepted a 50-ft drop test as an acceptable MoC in their Special Condition VTOL regulations [3]. The details in this MoC, which are based on existing fuel tank requirements for rotorcraft [4] require the ESS be drop tested from a height of 50 feet enclosed in surrounding structure and charged to its most critical condition. When examining the results from the test, the MoC states in the requirements "*the structural damage should not lead to fire; or if a fire should occur, the fumes or gasses should be contained for at least 15 minutes in non-occupied areas and outside the evacuation path."*

A team within the Revolutionary Vertical Lift Technology Project (RVLT) located at NASA's Langley Research Center has been undertaking a multi-year effort to conduct research on ESS in order to collect data to help in discussions regarding regulatory development. The test series described herein is the second in a three-phase series which intends to examine the response of ESS components under various configurations. In the first phase of testing, ESS modules were subjected to a 50-ft drop test under various orientations *without structure* to identify several fundamental factors. These factors included what types of various failures could be introduced (if any) into the modules during an impact event, and whether these

types of failures could be correlated to factors regarding loading levels, orientations, and other variables. Additionally, the data obtained could be used to identify correlations to cell level destructive testing.

One of the other objectives of the first phase of testing was to evaluate, to the best extent possible, the response of the ESS modules subjected to the tested conditions. While the modules were tested without supporting structure or external connections, which is a non-standard aircraft installation, instances where the modules could be subjected to loads without any type of significant attenuation present could arise. Since the tests were vehicle agnostic, there was no specific instance identified, and the modules were tested in various orientations in order to cover several potential instances. Finally, the information obtained was to be used to guide subsequent rounds of testing. The results from the Phase 1 testing are documented in refs 5 and 6, but are summarized for completeness.

In general, for Phase 1, the modules experienced large amounts of deformation, which led to a variety of internal failures in the cells, containment structures and electronics. The accelerations were of very high magnitude, ranging between 500 g and 1,500 g, with extremely short durations, typically only a few milliseconds. These levels more closely represented shock type loads and were out of family with accelerations levels typically seen in vehicle crash testing [7]. Two orientations experienced significantly larger amounts of damage and it was determined that orientation played a key role in the amount of damage measured. Additionally, a scoring rubric was developed to compare the type and amount of damage between the tests such that a quantitative metric or score could be produced and used as methods to compare the various tests conducted.

The Phase 2 testing, which is described herein, builds off Phase 1 testing by utilizing the information obtained from Phase 1. Noting the differences in results obtained in the scoring rubric, the orientations for Phase 2 configured the modules in the two highest scored orientations from Phase 1. Since the tests were still vehicle agnostic, items for surrounding structure were not addressed; however, attenuated loads representing generic deformation in the vehicle structure were added as a test condition. Thus, the idea of using an attenuated input pulse into the test condition was evaluated to simulate the *within structure* condition. Several example cases from rotorcraft [8] and eVTOL [9] tests conducted at NASA were examined to determine appropriate input levels. For the tests, two input conditions and orientations were selected and used.

Test Articles

The test articles were Electric Power Systems (EPS) Electric Propulsion Ion Core (EPiC) modules capable of providing 2.3 kWh of power, which were the same make and type of modules utilized in Phase 1 testing. All modules were designed to withstand TSO-179b [10] and UN 38.3 [11] requirements and, in an aircraft installation, intended to be connected together in conjunction with several other supporting components to form a Pack-level system. However, for this testing, individual modules were utilized as the test articles, and these individual modules were configurated to a zero-state-of-charge (ZSOC) condition. This condition minimized (but did not eliminate) the threat of a Thermal Runaway (TR) hazard and was chosen to maximize the chances that post-test teardowns and forensics could be conducted on the modules to determine internal damage and other observable parameters. Additionally, even at a low hazard probability, a ZSOC condition allowed for electrical and internal cell temperature and voltage information to be interrogated from within the module to determine generalities on the module connectivity and health. This information was collected via a handheld monitoring device supplied by EPS. A picture of the EPiC module is shown in Figure 1.

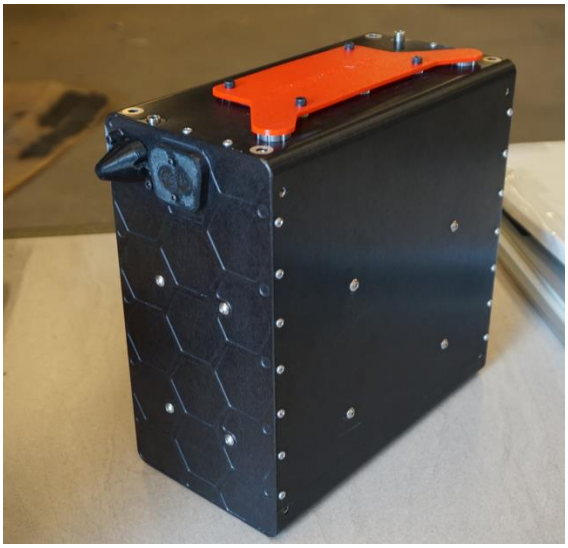

Figure 1. EPS EPiC ESS module test article

Note the test article has several protective coverings in the figure, which were removed prior to testing. Additionally, battery management systems, cooling lines and other electrical and mechanical hardware typically associated with an installed condition was not included in the test setup. Instead, the test setup limited the test article to the module only, which was similar to how tests were conducted in Phase 1.

Test Setup

For the tests, the modules were rigidly attached to the top of a rigid plate via custom mounting brackets. They were rigidly attached such that the accelerations at the plate were felt at the module level. The plate contained 12-in. long corner posts at each of the corners to allow for the lifting attachment locations to be above the center of gravity (CG), which provided a stable lifting and free fall conditions. The modules themselves were surrounded by rigid members which were intended to protect them from secondary impacts from the lifting cables or other test equipment and components, along with protecting the module in the event of the plate tipping over. Several items of ballast were attached on the outer portions of the plate to adjust the weight necessary to achieve the acceleration levels required. Finally, several brackets were added to the edges of the plate to act as edge stiffeners due to the expected bending of the plate during impact. These brackets also contained the yellow and black “bowtie” markers used for photogrammetry marker tracking.

To generate the required input pulse into the test article, stacks of crushable paper honeycomb pads were attached to the bottom of the plate. The pads were designed to produce desired loading levels through the controlled crushing of sequentially stacked layers by slightly increasing the crush area as the crush sequence progressed. Since the crush strength of the paper honeycomb was known, several pulses could be generated by only changing the geometry of the stacked pads. The test setup with components labeled is shown in Figure 2.

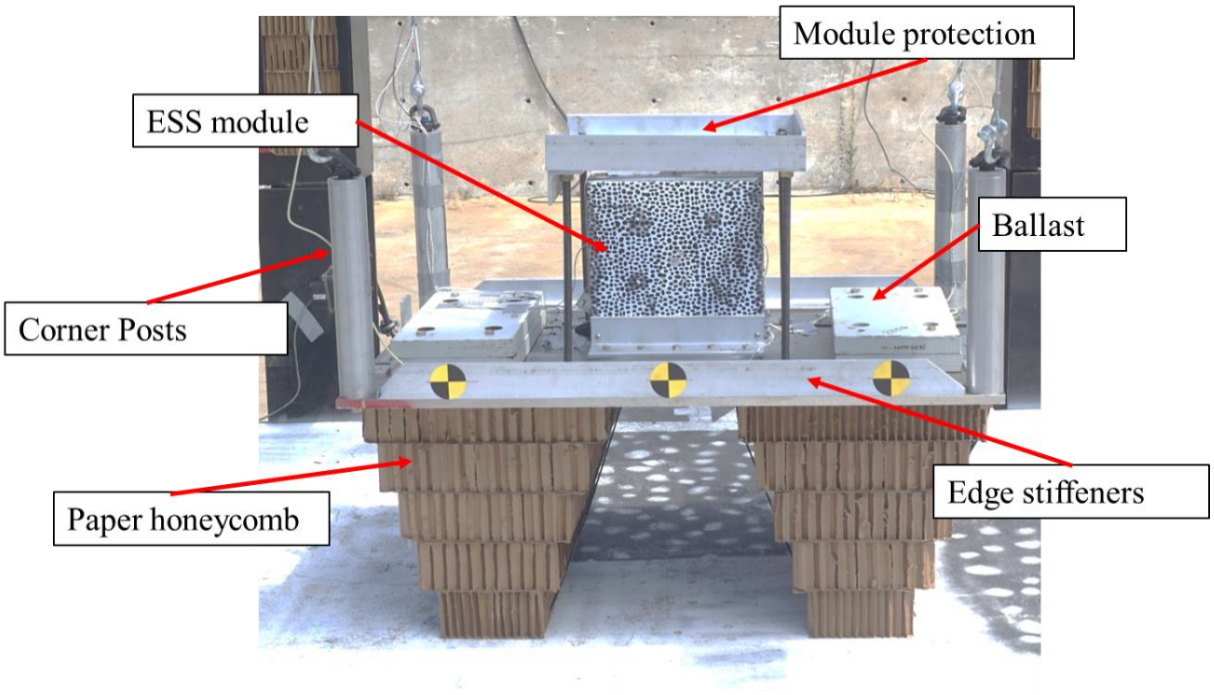

Figure 2. Test article configuration

All tests were conducted at the National Institute for Aviation Research (NIAR) outdoor drop facility, by NIAR personnel utilizing guidelines and methods previously developed by NASA [12]. The NIAR drop facility has been used for several ESS tests [13] and for the Phase 1 tests by NASA. The NIAR outdoor drop facility is shown in Figure 3.

Figure 3. NIAR outdoor drop facility

The test article was placed on the impact surface and connected via cables to the drop trolley. After checkouts were completed, the trolley was lifted such that the test article was at a height of 50 feet above the impact surface. After a countdown, the test article and trolley were released and travelled downward via guiderails. At the end of the fall, the test article impacted the rigid impact surface after which the cabling between the trolley and test article became slack, which decoupled the test article and trolley motion. The trolley motion was stopped by its own attenuation system and came to a rest above the test article shortly after impact.

After each test, the test article remained in its post-test condition for one hour under active observation to determine whether the test article was unstable and whether TR was imminent. After the hour of active monitoring, test personnel approached the test article and started the post-test inspections, which included visual and onboard connectivity and health monitoring. After the post-test inspections, the modules were removed from the plate and placed into outside storage for passive monitoring for 24 hours. The outside storage is shown in Figure 4.

Figure 4. Test articles in outside storage

Sensors included both accelerometers and thermocouples. For each test, two accelerometers were placed on the module itself at locations in the middle of the upper facing side and at the northeast corner. Two accelerometers were also placed on the plate. These accelerometers were typically on the south and east sides of the plate and did not change during testing. Since the connection between the module and plate were assumed to be rigid, comparisons between the plate response and the module response could be made to verify these assumptions.

Four thermocouples were placed in various locations on the modules. As with Phase 1, the thermocouples were placed on unpainted faces around the module, however, specific locations were not tightly controlled. The thermocouple data were intended to collect temperatures at various locations around the modules to check for a TR event. A portion of the instrumentation suite is shown in Figure 5. Note only half of the instrumentation is visible in the figure.

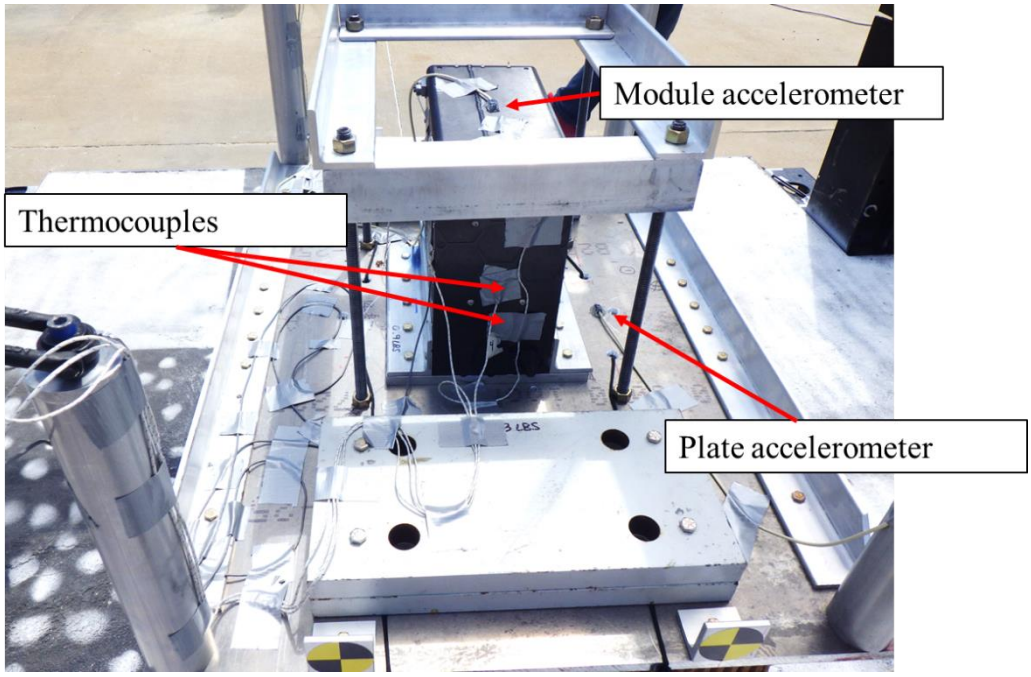

Figure 5. Test sensor instrumentation

Along with the sensor data, each module was captured with high-speed photogrammetry during the tests. Two techniques were utilized in the acquisition of the photogrammetry data, Digital Image Correlation (DIC) and marker tracking. To facilitate the acquisition of the DIC data, two sides of each module were painted with a black and white stochastic speckle pattern. To facilitate the acquisition of marker tracking data, yellow and black bowtie markers were placed on the drop trolley and on the stiffening structure on the plate, as previously mentioned. The high-speed photogrammetry was acquired utilizing Photron FASTCAM SA-Z high speed cameras, with a sensor resolution of 1024 pixels x 1024 pixels (1 mega-pixel, MP) and a frame rate of 10,000 frames per second (fps). Additional high-speed cameras were utilized on the non-DIC sides as general test views.

All accelerometer and temperature sensor data were connected to an offboard data acquisition system (DAS), sampling data during the test at 100 kHz. After the test was completed, the test data were saved, and the DAS began to monitor and record thermocouple data at a rate of 0.2 Hz. After the hour monitoring period was completed and the thermocouple data were saved, the post-test inspections began. After the post-test inspections, disassembly of the test fixture began, and a new module was installed in preparation for the next test. This process was repeated for all tests conducted.

Development of the Test Matrix

Several factors were considered when developing the test matrix for the Phase 2 testing. Since there were only three modules available to test, several tradeoffs were considered to maximize the impact of data collected. As previously stated, the modules used as the test articles were identical to those used in Phase 1 with the exception that the third module for Phase 2 was a spare module from Phase 1 and was not capable of providing onboard connectivity and health monitoring measurements. This module deficiency factored into the variables considered in the test matrix development.

One major constraint identified in the test conduct sequence was that post-test module disassembly and detailed forensics would not be available immediately after each test was completed. Instead, the detailed forensics of the modules would occur offsite and at a later date, which meant that comprehensive knowledge

on the internal structural deformation(s) was not available other than its effect (if any) on the data capable of being measured from the connectivity measurements immediately after each test. This constraint led to decisions on subsequent tests only being based on the knowledge obtained from the onsite visual inspections, acceleration levels, thermocouple data and the immediate post-test handheld monitoring results.

The starting point for the matrix utilized the results from Phase 1. Three ideas were considered: testing the orientations producing the two lowest rubric scores, testing the lowest and highest rubric scores, and testing the two highest rubric scores. After consideration, the decision was made to develop the test matrix to reflect tests that could show how much improvement could be made in the rubric score by retesting the highest scored orientations from Phase 1. A full description of the rubric is provided in the *Overview of the Scoring Rubric Section* of this report.

Considerations were next given to the order of the tests. One idea was to test the highest scored orientation at a predetermined loading level and evaluate the results. If the indications pointed to no damage in the test article, then the test would be repeated at a higher level. If damage was indicated, then the test would be repeated at a lower level. However, the repeat test would have to be conducted on the spare module knowing that post-test connectivity monitoring results would be unavailable, thus complicating the results. Another idea was to test the second highest scored orientation, determine its survivability, test the second highest orientation at a higher level using the spare module, and then test the final module in the highest orientation. There were several other options also considered for the order.

In the end, it was decided to test the second highest scored module at a predetermined loading condition. If this module survived, then the highest scored module would be tested at the same loading condition. If the second module survived, then the highest scored module would be retested at a higher loading condition using the spare module. This test matrix allowed for several factors to be addressed. The first was to determine whether it was possible to improve survivability for a number of (in this case two) orientations, which gave two distinct comparisons to the Phase 1 test results. The second was to determine thresholds of survivability for at least one of the orientations utilized. This would allow for three comparisons to be made (Phase 1, Phase 2 loading condition, Phase 2 higher loading condition). In this respect, the three tests selected allowed for multiple comparisons to be completed. The full test matrix decision tree is shown in Figure 6.

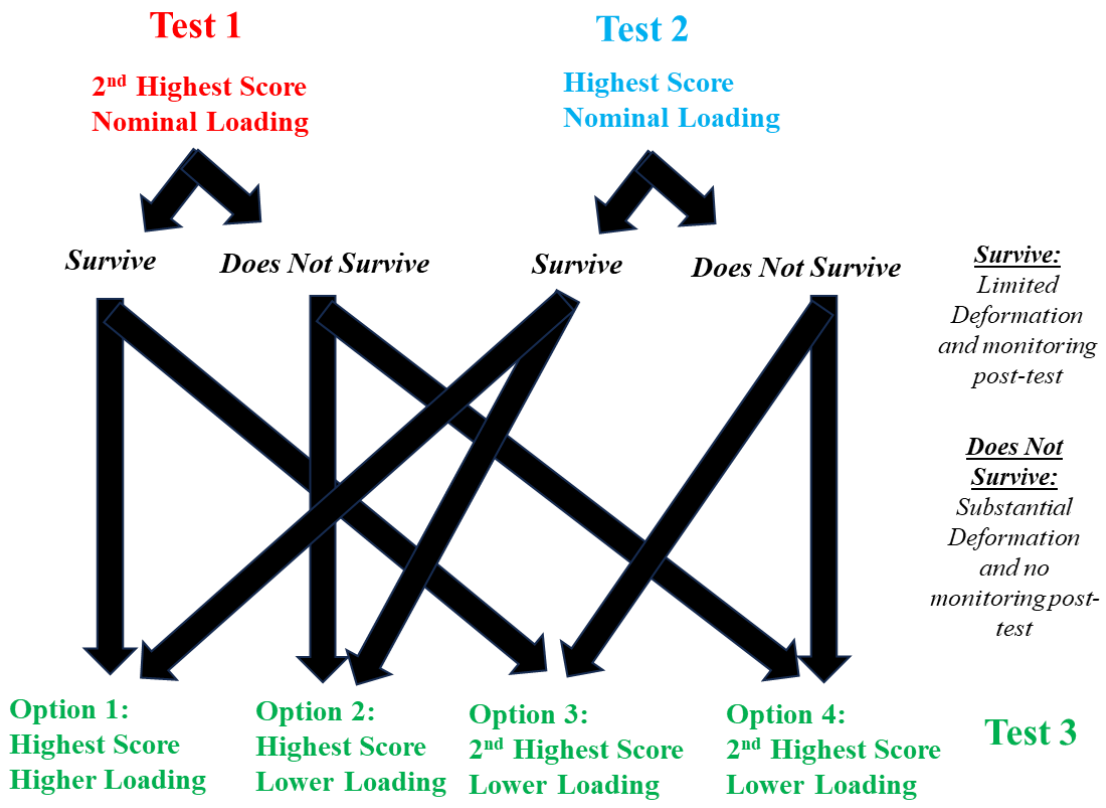

Figure 6. Test Matrix Decision Tree

The final decision that was made was to determine loading levels for the tests. Three values were needed: a nominal input acceleration, a higher input acceleration, and a lower input acceleration. As previously stated, several full-scale crash tests were utilized in developing the input accelerations into the test articles. These tests were evaluated against the constraints of the paper honeycomb used to generate the pulses, and the specific magnitudes emerged.

Data were sampled from two tests of small VTOL vehicles. The first data set was from a recent Lift + Cruise (L+C) test conducted at NASA's Langley Research Center [9] in 2022. In this test, accelerations of over 140 g were measured at the belly and between 40 g and 60 g at the floor level. An earlier NASA test conducted on a small MD-500 helicopter in 2010 [8] measured accelerations of approximately 40 g at the floor level. The eventual level settled for the nominal loading pulse was 80 g in magnitude. This magnitude was chosen because it was within the range of what was collected from full scale testing, but also approximately double to what could be expected at the floor locations which would be the levels experienced by the onboard occupants and would envelope any of the occupant response. The lower level chosen was a 40-g level, which was half of the nominal pulse, but also the same approximate value as the floor level loading for both of the tests. The higher level was chosen to be approximately double the nominal pulse, but constraints in the paper honeycomb and ballast available increased the final magnitude of this pulse to almost triple the nominal pulse, to 220 g.

Overview of the Scoring Rubric

The scoring rubric was again used during the post-test forensics inspections which occurred at the EPS facility several weeks after the testing was completed. The rubric is discussed in detail in ref 6 but is summarized here for completeness. Since the modules were in a ZSOC configuration, the actual damage

produced from the tests in an installed module were not able to be determined. Thus, commentary on the threat of TR or the hazards developed from shock created by testing in various configurations cannot be inferred from the results of the drop tests. Instead, the rubric was used as an alternate method to measure and compare the differences in module response. This scoring rubric utilizes the results obtained from the forensics inspections at two levels: the Assembly level and the Cell level. At the Assembly level, three components were identified as the subjects to be inspected. Moving from the inside going to the outside starting with the cells, the three assemblies were identified: the Cell Assembly, the Containment Assembly, and the Enclosure Assembly. These were all inspected for damage and given ratings of "Low", "Medium", "High", "Severe" which corresponded to numerical values between 1 (Low) and 4 (Severe). In addition to the value itself, each assembly was weighted according to its proximity to the cells, with the Cell Assembly receiving a multiplier of 3 being the closest to the cells, the Containment assembly receiving a multiple of 2, and the Enclosure Assembly receiving a multiplier of 1 being the furthest away.

At the Cell level, interrogations into the each of the individual cells were used as the basis of the score. Each of the cells were examined for damage in three categories - Pouch Puncture, Pouch Breach, and Pouch Deformation. Pouch Puncture and Pouch Breach were differentiated by cause of the damage - puncture was due to an external object penetrating the cell while breach was due to the inertia of the cell itself. The cell damage numbers were also weighted with multipliers which were based on the damage severity. A fourth category recorded the number of electrical shorts in the cells, both in the cells themselves and in the cell to the enclosures. Finally, the presence of electrolyte smell was included and was based on a binary yes/no value depending on whether it was detected or not. The rubric, in table form, is shown in Table 1.
.

Table 1. Scoring Rubric

Assembly Level Damage	Severity	Multiplier	Score	Notes
Enclosure Assembly	Low (1)	1		
	Medium (2)			
	High (3)			
	Severe (4)			
Containment Assembly	Low (1)	2		
	Medium (2)			
	High (3)			
	Severe (4)			
Cell Assembly	Low (1)	3		
	Medium (2)			
	High (3)			
	Severe (4)			
Cell Level Damage	**# Cells**	**Multiplier**	**Score**	**Notes**
Pouch Puncture		10		
Pouch Breach		10		
Pouch Deformation		4		
Electrical Shorts		3		
Electrolyte Smell	Yes / No	10		

Once the inspections recorded all the values into the rubric table, the values from the Assembly and Cell levels were tallied and compared between each test.

Test Results

Test 1 - Upside Down Orientation at the Nominal Loading Condition

The first test was conducted using the 2nd highest scored module from Phase 1 in the nominal loading condition. This configuration oriented the module upside down and subjected it to the 80-g nominal acceleration. The test was conducted on June 26, 2024, at 12:11 PM local time. The temperature was 92.9° F with winds calm. The test article impacted at the north-east corner, with a north-side low angle of 3.0 degrees, east-side low angle of 0.6 degrees and an impact velocity of 54.2 feet per second (ft/s). An image sequence is shown in Figure 7.

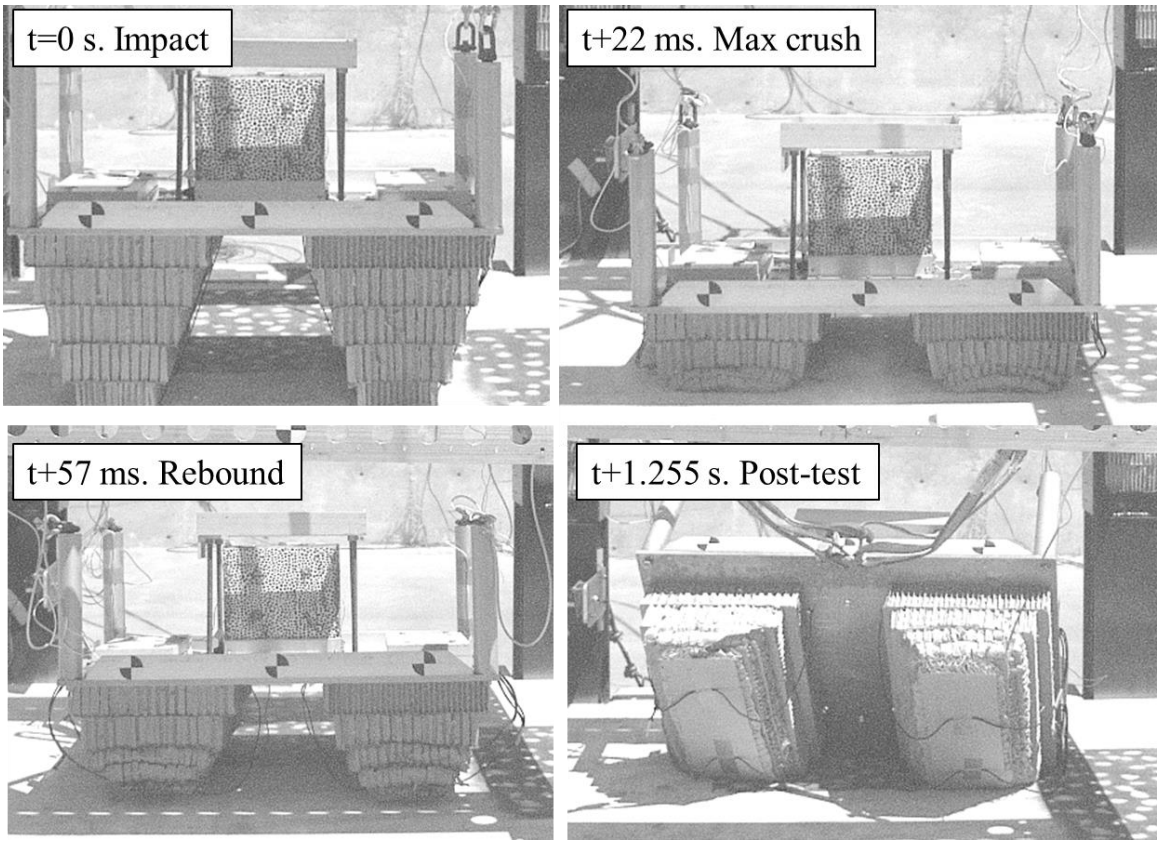

Figure 7. Upside Down test sequence

There are four images presented in Figure 7 which depict the test sequence. The top left image shows the test article with ESS module at impact. The top right image shows the paper honeycomb pulse generator at its maximum crush distance with little deformation developed in the plate or ESS module. The lower right image is after the time of maximum crush and at a time where the test article has rebounded off the impact surface. The lower right image is the test article at rest, post-test. The test article ended up partially on its side, tipping away from the view shown in the figure due to the south-side high impact attitude. It ended on its side due to a slight angle at impact, which resulted in minor differences in the forward-to-backward paper honeycomb crushing. However, the ESS module was unaffected by this post-test orientation since it had protection from both the surrounding structure and corner posts. The test article, in its post-test position, is next shown in Figure 8.

Figure 8. Upside Down test article post-test pictures

There did not appear to be any visible damage on either the ESS module or the plate and its various components. Other than the crushing of the paper honeycomb, the test article appeared to be undamaged by the impact. Post-test health check measurements of the module were conducted using the handheld monitor while the module was still mounted to the plate post-test, and the measurements were nominal. The data were collected, saved, and plotted. The accelerations measured on the plate and the ESS module are first shown in Figure 9.

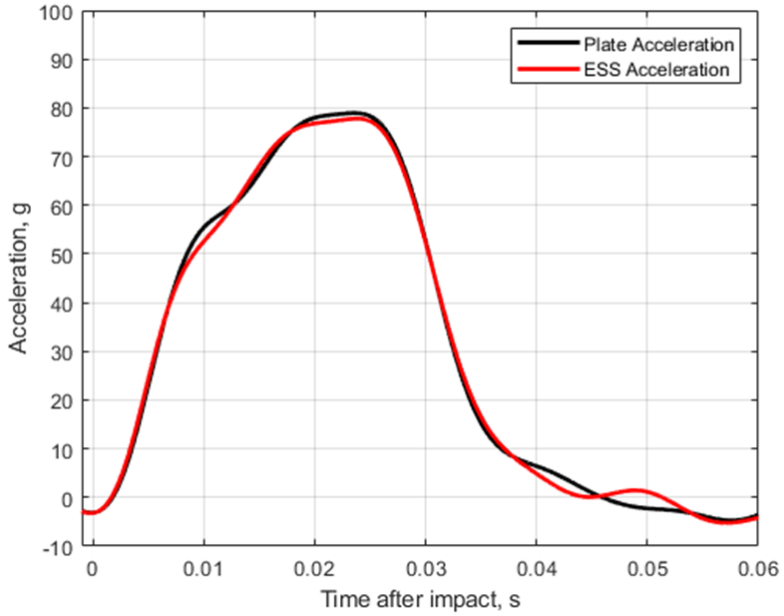

Figure 9. Upside Down test acceleration

The accelerations measured in the plate and in the module confirm the rigid connection between the two since the measured values closely match one another, both in magnitude and in shape. The peak magnitudes of the of acceleration were 78.9 g for the plate and 77.7 g for the module, which were only very slightly below the 80-g expected magnitude. Both pulse shapes were approximately 45 milliseconds (ms) in duration and resembled a half sine shape. The peak magnitudes occurred 23 ms after impact, which corresponded to the time of maximum crushing in the paper honeycomb shown in Figure 7. Next,

temperature data were examined for the immediate impact time, but also for the hour post-test monitoring time. The temperatures measured during the impact are first plotted and shown next in Figure 10.

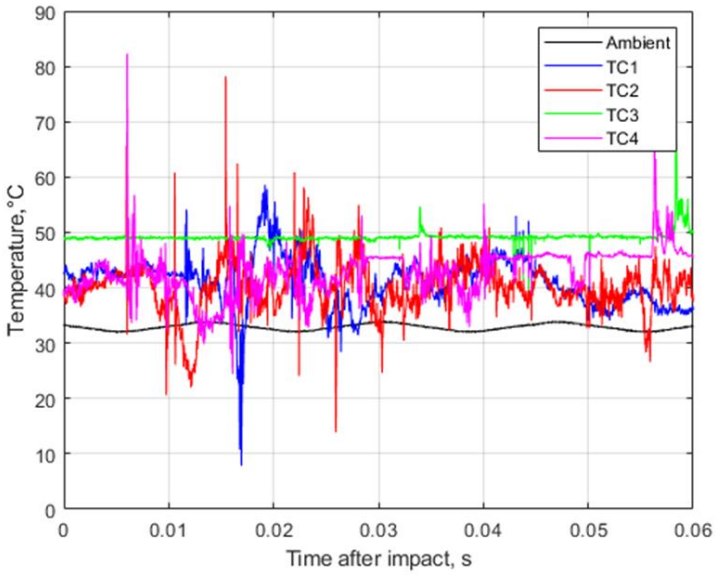

Figure 10. Upside Down test temperatures

The temperature data plotted in Figure 10 contains all of the thermocouple data (denoted as "TC" in the figure) along with the ambient temperature. The thermocouple data are plotted along the same timescale as the accelerations, so direct comparisons between timing events could be investigated. While there were spikes that occurred during the impact event, there was nothing in the temperature data to suggest an uncontrolled temperature rise, which is an indicator for TR. The post-test hour long temperature monitoring data is next shown in Figure 11.

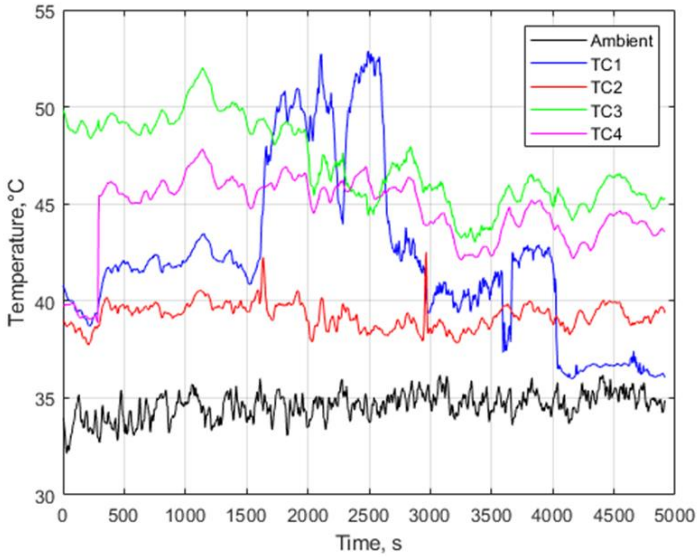

Figure 11. Upside Down post-test temperatures

The post-test monitoring of the temperatures on the module produced various increases and decreases but did not show uncontrolled temperature rise in any of the locations monitored. Thermocouple 3 (TC3) measured a mainly downward temperature trend, while thermocouple 4 (TC4) measured a generally flat trend. There were jumps in the data for thermocouple 1 (TC1), which could be indicative of a sunny to

cloudy transition, creating additional temperature on the upward facing side, or could be measuring a potential shadow from the trolley due to the changing sun position. Since the locations of the actual thermocouples were not tightly controlled, the locations were not definite so no definitive conclusions can be made. However, there was no trend present showing a temperature rise, suggesting uncontrolled heating, which is a sign of TR. The deformation in the module was next examined. The full-field digital image correlation contour plots of the in-plane and out-of-plane deformation are next shown in Figure 12.

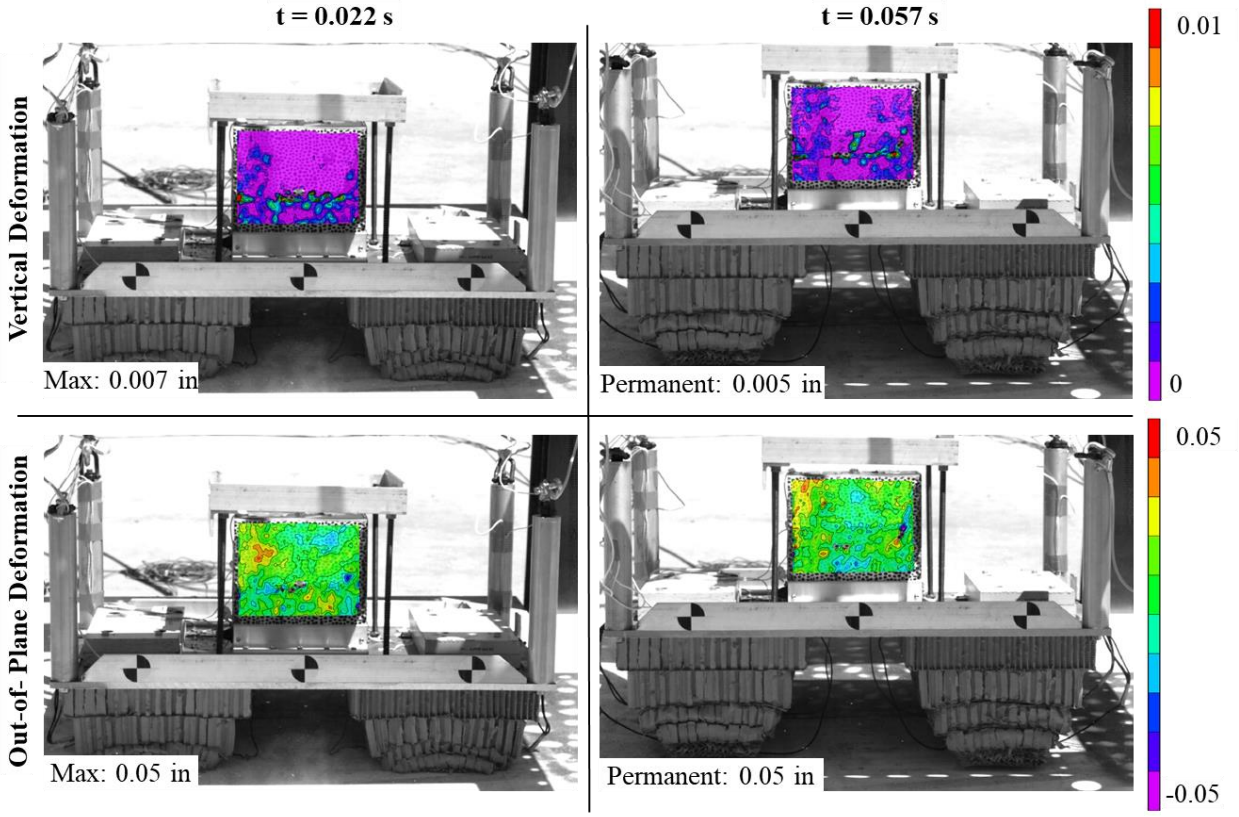

Figure 12. Upside Down in-plane and out-of-plane deformation contour plots

It can be observed in the figure that the maximum, localized in-plane (vertical) and out-of-plane deformation of the module was approximately 0.007 in. and 0.050 in., respectively, during the impact event (at maximum crush, t = 0.022 s) and subsequent rebound, t = 0.057 s. Note the localized "hot spots" were more than likely related to surface artifacts on the module (i.e. fasteners and standoffs) and/or shadows from the drop trolley and equipment, resulting in correlation issues. Next, the time-history of the average displacement, as measured across the entire surface of the module, is shown in Figure 13.

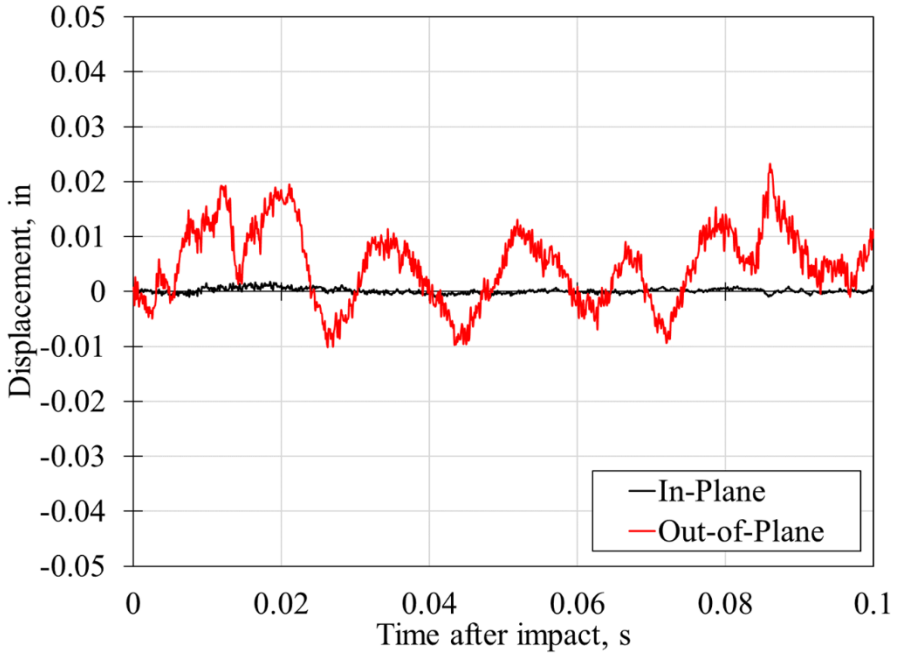

Figure 13. Upside Down in-plane and out-of-plane displacement time-history plots

The average in-plane (vertical) deformation was approximately ± 0.002 in, while the average out-of-plane deformation was approximately ± 0.015 in. The axial (vertical) strain of the module, measured using a virtual extensometer across the left edge, center and right edge of the module, is shown in Figure 14. The overall strain response of the module was identical across the surface and ranged between approximately ± 1000 με.

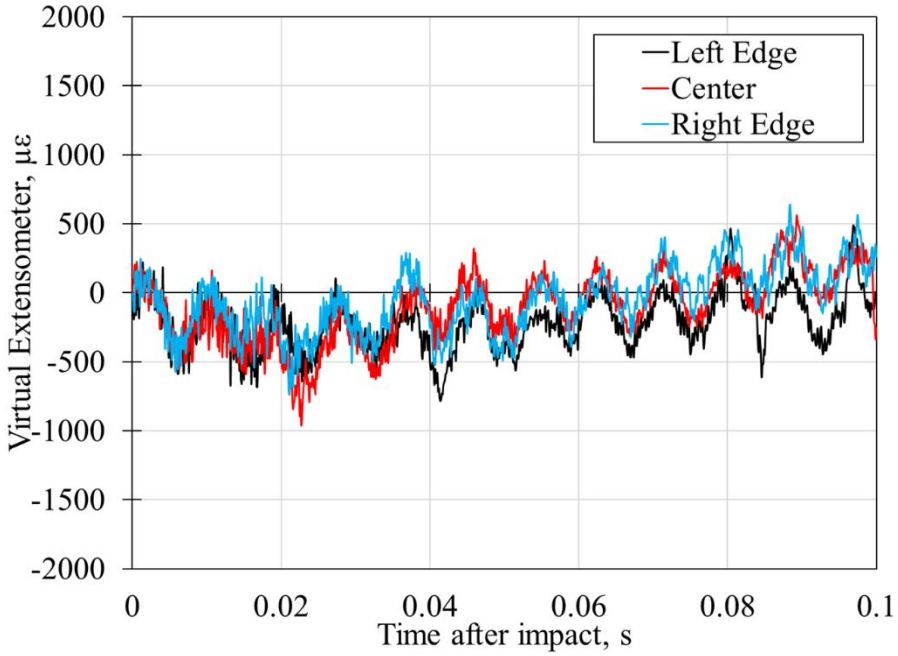

Figure 14. Upside Down virtual extensometer time-history plots

After the test, the module was removed from the test site, and post-test inspections occurred. All post-test inspections for all three test articles occurred at the EPS hangar on July 29, 2024. The inspections for the

Upside Down module revealed little internal damage. After the Enclosure Assembly was removed, it was noticed that there was a very slight inward deformation from the standoffs at the top of Containment Assembly near the top vent port. The end view of the module is shown in Figure 15, noting the Cell Assembly is shown on the forward face. The Containment Assembly is still wrapped around the other faces of the module.

Figure 15. Upside Down Cell Assembly (forward face) and Containment Assembly (other faces)

The deformation of the Containment Assembly was very minor and difficult to notice in Figure 15. The largest noticeable feature can be observed by examining the upward facing standoff near the top right of the figure, which was oriented slightly inward. The Containment and Cell Assemblies were next removed in order to examine the cells themselves. The cells are next shown in Figure 16.

Figure 16. Upside Down cells

The cells appeared to be undamaged from the impact. There were no noticeable deformations or breaches nor was electrolyte smell noticed. The post-test inspections gave the module assembly scores of "low" for the Enclosure and Cell assemblies, and a "Medium" for the Containment assembly due to the standoff deformations. There did not appear to be any physical damage to the cells, so the cell damage assembly scores were zero. When compiled, the rubric produced a final score for the Upside Down test of 8. The Sideways test at nominal loading was the next test conducted and is presented next.

Test 2 - Sideways Orientation at Nominal Loading Condition

The second test was conducted using the highest scored module from Phase 1 in the nominal loading condition. This configuration oriented the module sideways and subjected it to the 80-g nominal acceleration. The test was conducted on June 26, 2024, at 1:40 PM local time. The temperature was 93.0 F with winds calm. The test article impacted at the north-east corner, with a north-side low angle of 0.5 degrees, east-side low angle of 1.3 degrees and an impact velocity of 53.9 ft/s. An image sequence is shown in Figure 17.

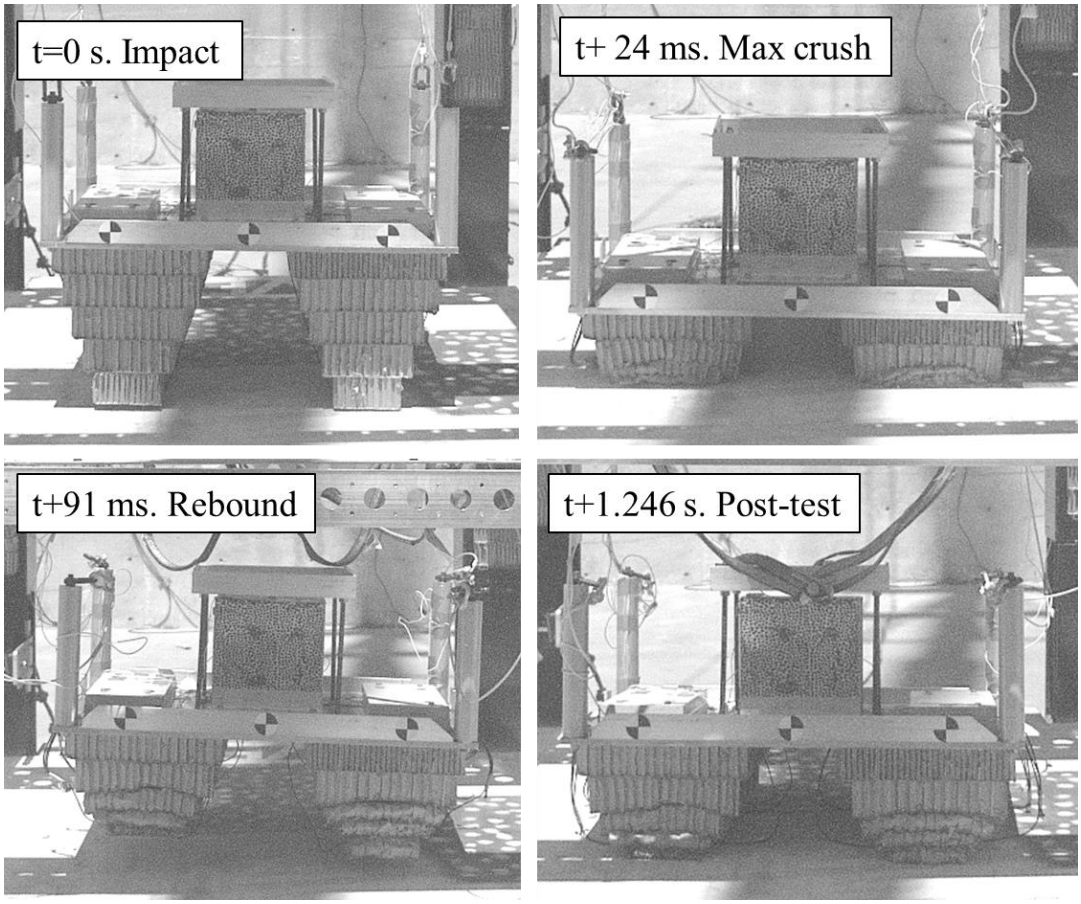

Figure 17. Sideways test sequence

The upper left image shows the test article at impact. Note the right stack of paper honeycomb has impacted the surface while the left side has not, indicating a west side high impact. The upper right image shows the test article 24 ms after impact, which is at the time of maximum honeycomb crush, which agrees with the timing obtained from Test 1. At 91 ms after impact, the test article has rebounded off the impact surface, which is shown in the lower left image, and came to rest 1.246 s after initial impact, which is shown in the lower right image. Unlike Test 1, the test article remained upright post-test. Post-test photos of the test article are next shown in Figure 18.

Figure 18. Sideways test article post-test pictures

As with Test 1, there did not appear to be any visible damage on either the ESS module or the plate when examining the post-test results. Using the handheld monitor, post-test health check measurements were able to be obtained on the module while still mounted to the plate post-test and were nominal, suggesting whatever internal damage that may have occurred did not affect the health check measurements. The accelerations obtained on the plate and module were next examined and are plotted in Figure 19.

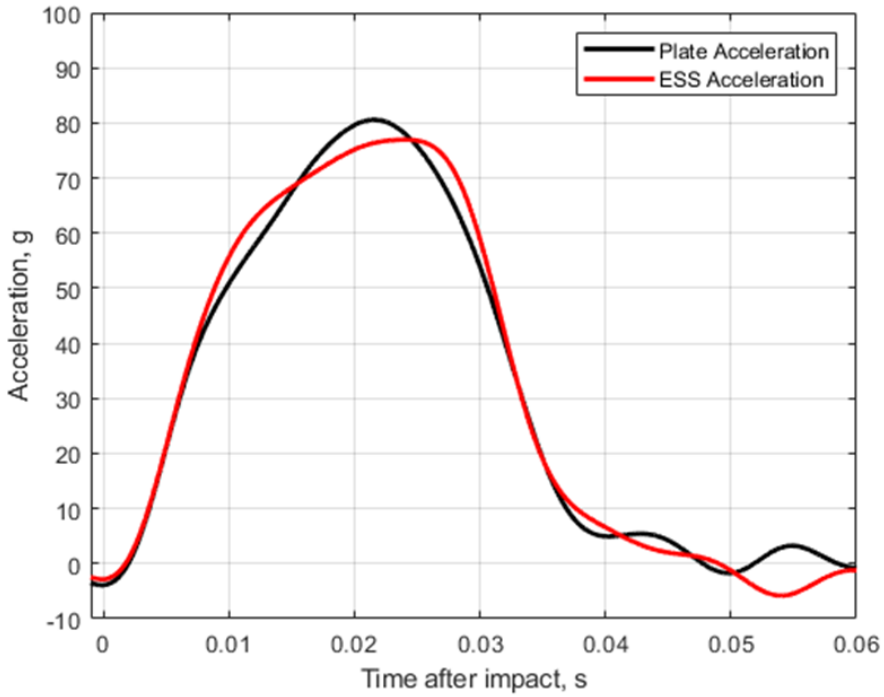

Figure 19. Sideways test acceleration

The acceleration on the plate reached a maximum value of 80.5 g, approximately 22 ms after impact. The acceleration measured in the module was slightly less, measuring 76.8 g approximately 25 ms after impact. These slight differences could be caused by slight deformations in the module itself or simply typical measurement scatter in the collected acceleration data. The accelerations from the other two accelerometers, which are not shown in the figure, also deviated slightly from the presented curves,

suggesting minor differences in accelerations in the measured locations. The differences were attributed to normal test variation, and the data were close enough to the expected nominal value, that further investigations into the differences were not conducted. Unfortunately, no temperature data were collected during the impact due to a data system triggering issue. However, the temperature data from the post-test monitoring was collected and is shown next in Figure 20.

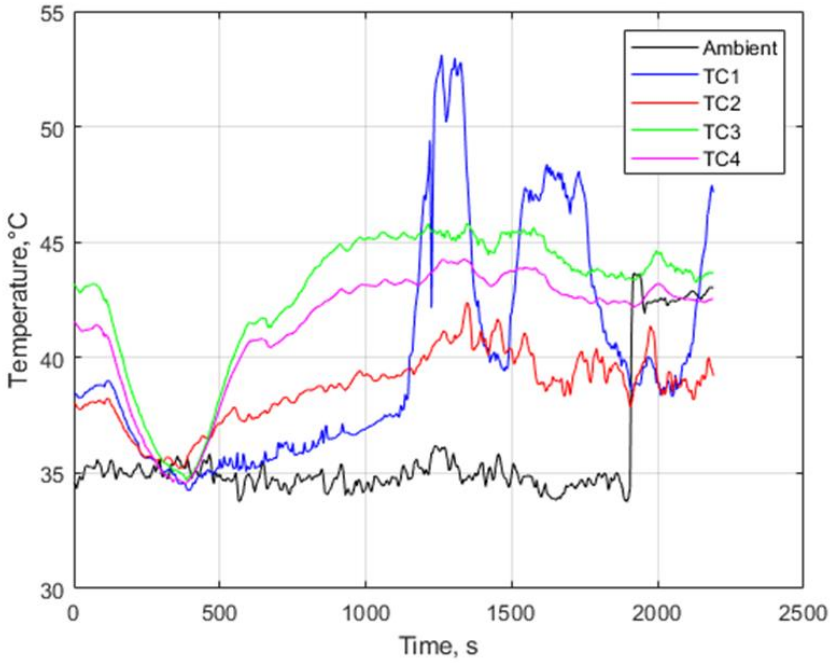

Figure 20. Sideways post-test temperatures

The post-test monitoring of the temperatures on the module showed both increases and decreases in temperatures. There was a noticeable decrease in all of the thermocouple measurements almost immediately after the test, suggesting clouds or shadows covered the entire module, leading to uniform cooling during this period. After this period of cooling, the temperatures increased to pre-dip levels, and TC2-TC4 gradually increased until a plateau was reached. TC1 measured several distinct increases and decreases suggesting this thermocouple was being affected an external object. It was not determined what caused these plateaus to appear in the TC1 data, but it also seemed to appear in the ambient data toward the end of the monitoring, suggesting a possible global increase in temperature or some other type of unknown sensitivity in the data system. Even with these behaviors, the module did not appear to experience uncontrolled temperature rise. The deformation in the module was next examined. The full-field digital image correlation contour plots of the in-plane and out-of-plane deformation are next shown in Figure 21.

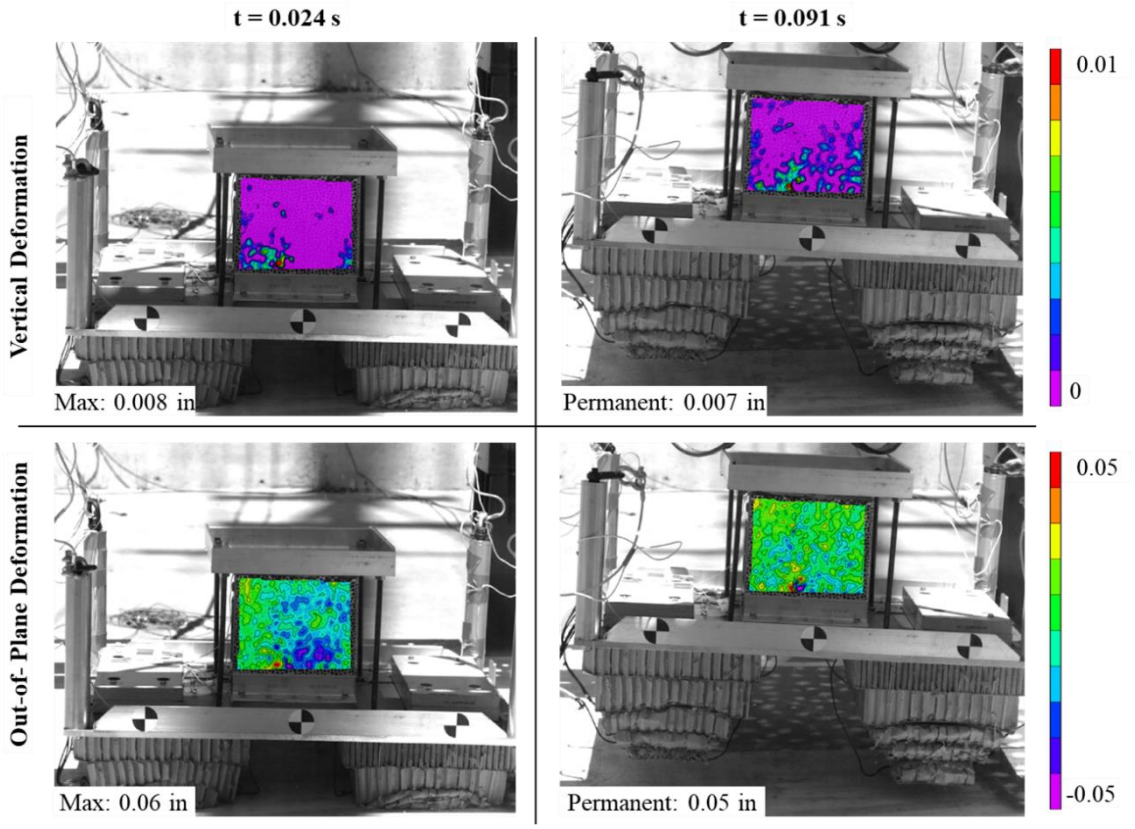

Figure 21. Sideways in-plane and out-of-plane deformation contour plots

It can be observed in the figure that the maximum, localized in-plane (vertical) and out-of-plane deformation of the module was approximately 0.008 in. and 0.060 in. respectively during the impact event (at maximum crush, t = 0.024 s) and subsequent rebound, t = 0.091 s. Note the localized "hot spots" were more than likely related to surface artifacts on the module (i.e. fasteners and standoffs) and/or shadows from the drop trolley and equipment, resulting in correlation issues. Next, the time-history of the average displacement, as measured across the entire surface of the module, is shown in Figure 22.

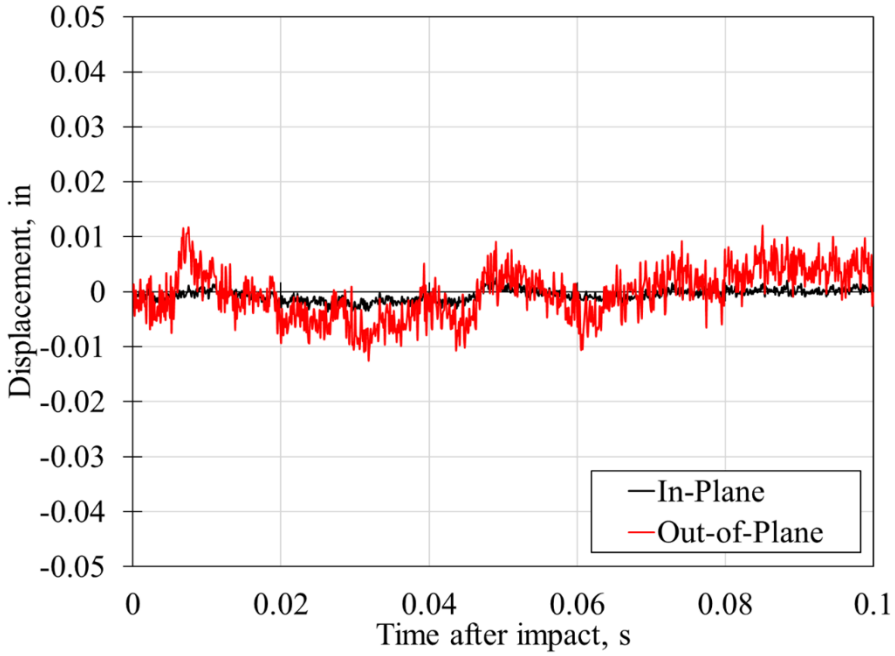

Figure 22. Sideways in-plane and out-of-plane displacement time-history plots

The average in-plane (vertical) deformation was approximately ± 0.003 in., while the average out-of-plane deformation was approximately ± 0.010 in. The axial (vertical) strain of the module, measured using a virtual extensometer across the left edge, center and right edge of the module, is shown in Figure 23. The overall strain response of the module was identical across the surface and ranged between approximately ± 500 με.

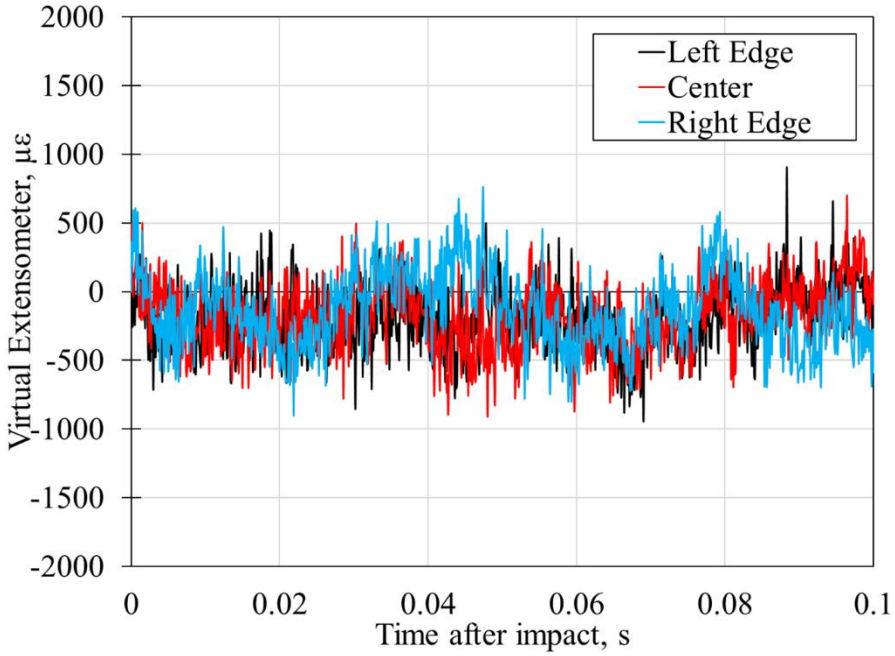

Figure 23. Sideways virtual extensometer time-history plots

After the test, the module was removed, and post-test inspections occurred. After the Enclosure and Containment Assemblies were removed, the Cell Assembly was revealed. The end view of the module is

shown in Figure 24, with the Cell Assembly observable on the forward face. The Containment Assembly is still wrapped around the other faces of the module.

Figure 24. Sideways Cell Assembly

The Cell Assembly appeared to be undamaged from the test. The assembly walls were undamaged after the test, and there was no orientation change in the standoffs. After the Cell Assembly was removed, the cells themselves were examined. The cells are shown next in Figure 25.

Figure 25. Sideways cells

There did not appear to be any visible damage from puncture, breach, or deformation, nor was there the presence of electrolyte. After investigations into the three enclosures and cells, the post-test inspections revealed little to no damage visible in the entirety of the module. The Enclosure, Containment and Cell Assemblies all received "Low" scores from the rubric. At the cell level, there was no sign of any cell damage, whether it be from puncture, breach, deformation, or the presence of electrolyte. These results led to a rubric score of 6, which is the lowest score possible.

After the second test was completed, all indications pointed to the conclusion that the test articles appeared to be undamaged from the tests (as a reminder, the post-test forensic inspection data were not available during the drop testing). It was decided the third test would be conducted using Option 1 from Figure 6, which was the highest scored module from Phase 1 subjected to the higher loading level. This configuration placed the module in the sideways orientation and subjected it to the higher 220-g loading level. This third and final test is described next.

Test 3 - Sideways Orientation at Higher Loading Condition

The third test was conducted using the highest scored module from Phase 1 in the higher loading condition due to the results obtained from tests 1 and 2. This configuration oriented the module sideways and subjected it to the 220-g loading acceleration. To achieve the higher acceleration, the plate was reconfigured by removing the ballast and utilized a different design of crushable paper honeycomb. All other parameters from the plate were unchanged from test two. The test was conducted on June 26, 2024, at 4:24 PM local time. The temperature was 92.8° F with winds calm. The test article impacted at the north-east corner, with a north-side low angle of 3.1 degrees, east-side low angle of 2.1 degrees and an impact velocity of 53.4 ft/s. An image sequence of the test is shown in Figure 26.

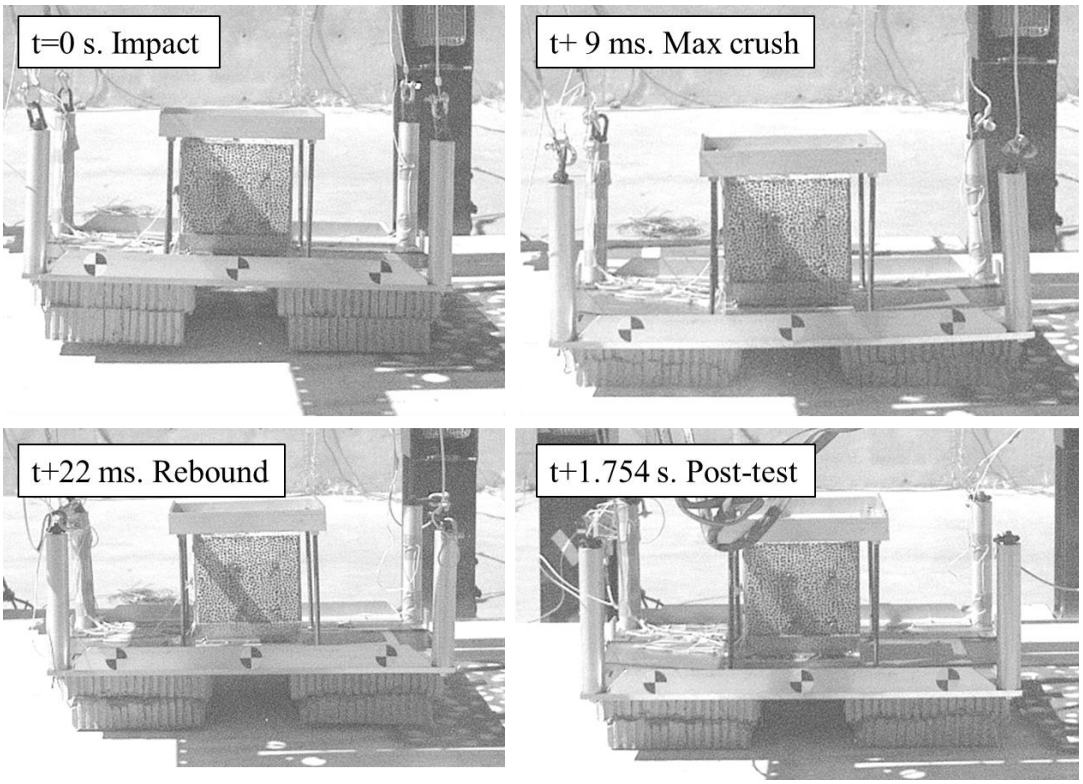

Figure 26. Sideways higher loading condition test sequence

The test article impacted the surface at West and South side high angles, which led to the Northeast corner of the plate making the initial contact with the impact surface. The maximum crushing of the paper honeycomb occurred 9 ms after impact, which is depicted in the upper right image in the figure, which is a significantly shorter time than the other two tests. The plate and test article rebounded 22 ms after initial impact and came to rest 1.754 s after impact. The module appeared to move rigidly with the plate motion and did not get impacted by any external object during the test. The module, in its post-test condition, is shown next in Figure 27.

Figure 27. Sideways higher loading condition test article post-test pictures

Visual inspections, post-test, showed no significant damage on the module or plate. Since this was the spare module, there were no post-test health check measurements obtained. The acceleration data from locations on the plate and module are plotted in Figure 28.

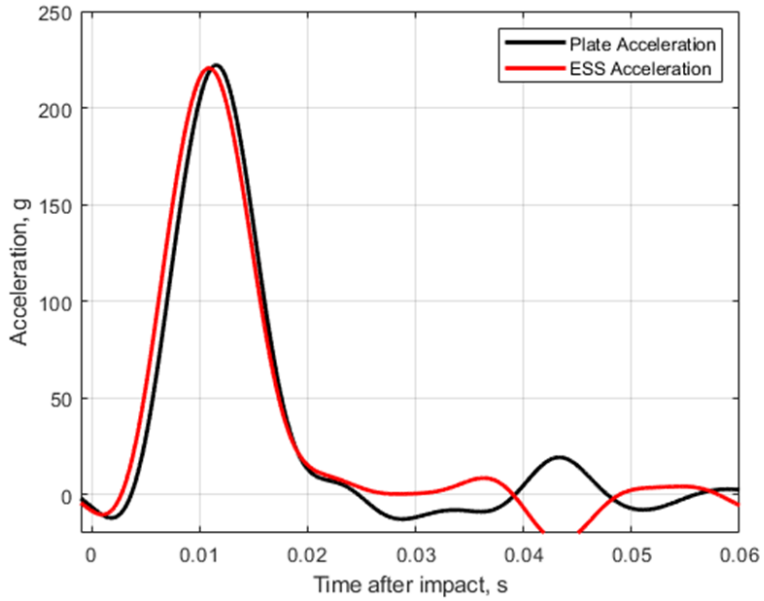

Figure 28. Sideways higher loading condition acceleration

The maximum values of acceleration were measured to be 222.1 g and 220.5 g on the plate and module, respectively. The time to peak acceleration was 10 ms to 11 ms, which was the approximate time of the maximum crush of the paper honeycomb, and less than half of the time for Tests 1 and 2. The curves matched closely throughout the event, however the acceleration on the ESS module was slightly ahead of the plate acceleration. This difference in time was less than 1 ms and determined to be a result of the different sensor locations in the test. There is a small bump in the acceleration data approximately 43 ms after impact, which was due to the large amounts of vibrations in the plate. High speed video confirmed there were no external contact with rigging hardware or other test components that would have caused this bump. The data from the thermocouples were next examined and are presented next in Figure 29.

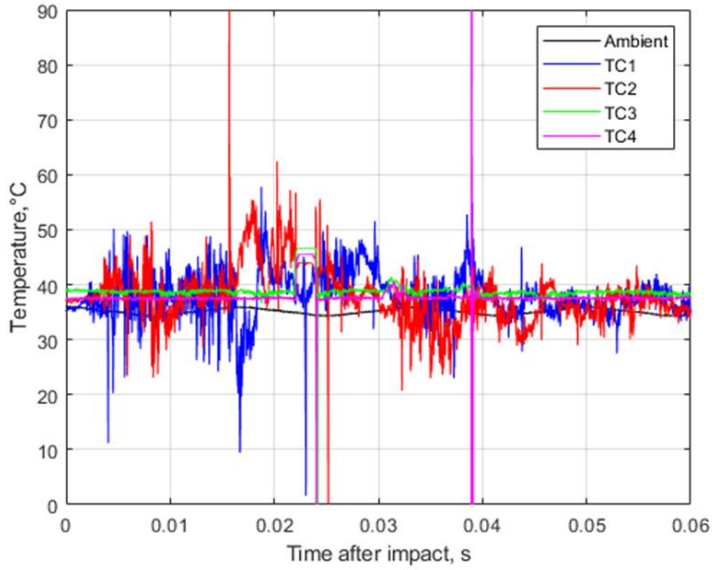

Figure 29. Sideways higher loading condition temperatures

When examining the thermocouple data as a whole, it appears to be relatively constant during the test, hovering between 30° C and 50° C. The large spikes in several of the thermocouples which last only for a single data point can be attributed to signal noise and were neglected during the data analysis. There was, however, short periods of temperature rise and fall which occur primarily before 30 ms and could be due to the motion or deformation of the ESS module. However, signs of uncontrolled temperature increase were not present, which pointed to the conclusion that TR was not occurring. The post-test monitoring temperature data were next examined and are plotted in Figure 30.

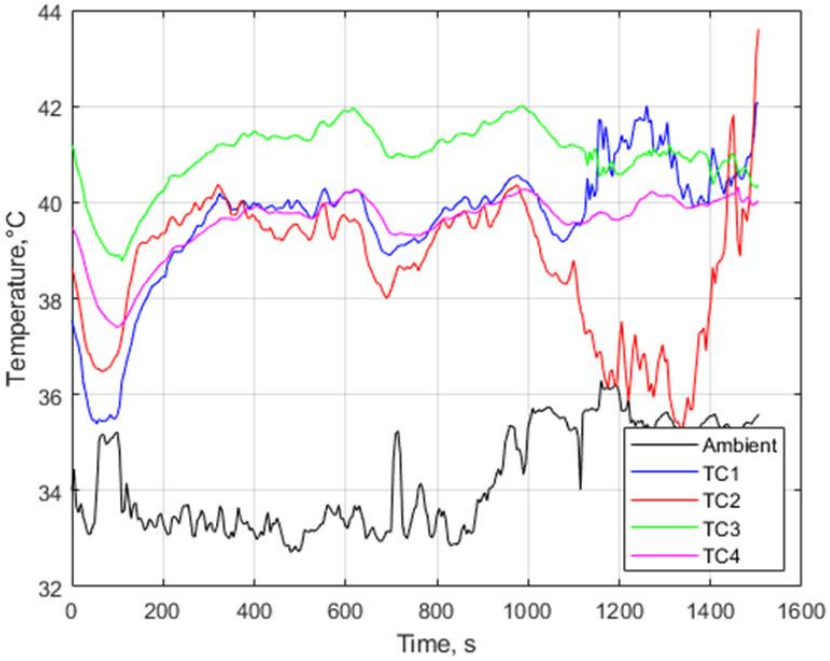

Figure 30. Sideways higher loading condition post-test temperatures

The post-test temperature data appeared to show similar trends to the data collected from Test 2. Early in the monitoring, there appeared to be a decrease then increase in all of the thermocouples attached to the module. At this same time, there appeared to be a slight increase in the ambient temperature. It is unclear whether these two items were related, however after this dip, the temperatures in the four thermocouples all increased until a plateau was reached. This plateau continued for the next 1000 s, after which TC1 and TC2 began to deviate. TC1 showed slightly increased temperatures reaching a slightly higher plateau, while TC2 started with a large decrease, then began to increase toward the end of monitoring. There was also an increase in the ambient temperature, which was unexpected since this test was conducted in late afternoon, in which the temperatures typically begin cooling. However, even with all of the thermocouple data presented, the module did not go into TR, and thus was removed from the test area after the 1-hour period and put into outside storage. The full-field digital image correlation contour plots of the in-plane and out-of-plane deformation are next shown in Figure 31.

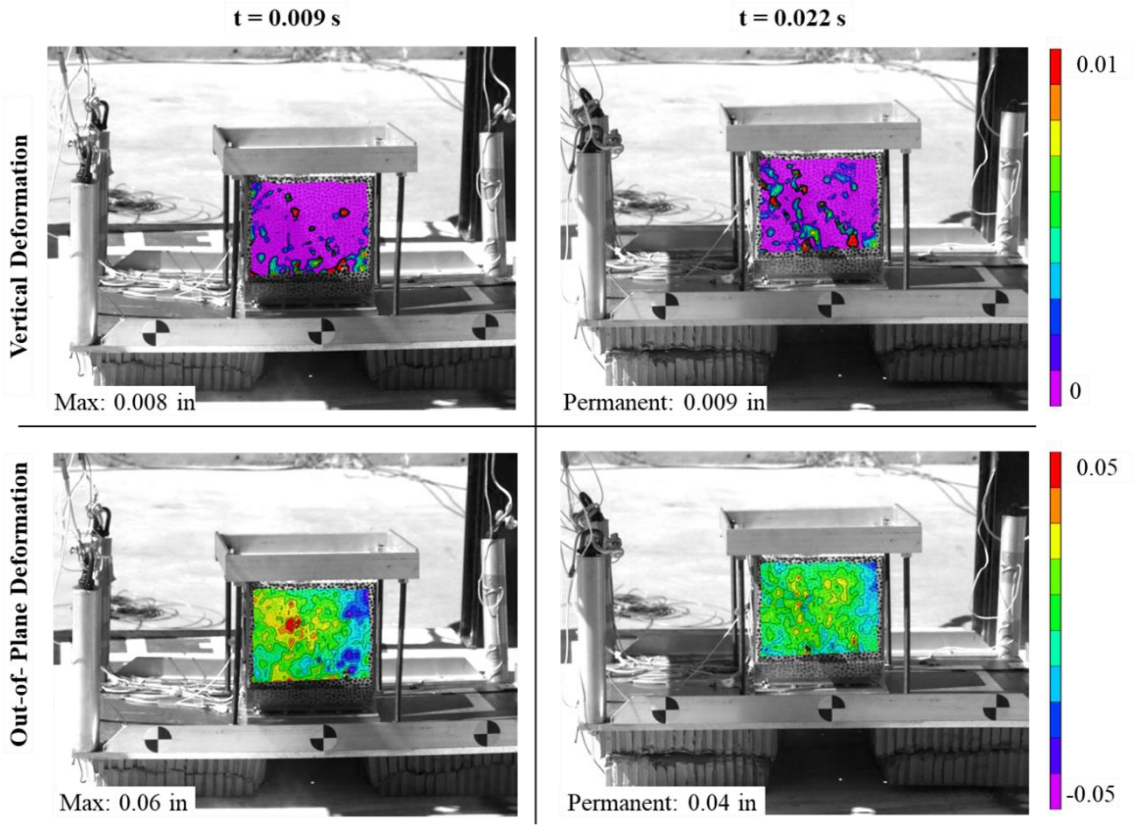

Figure 31. Sideways higher loading condition in-plane and out-of-plane deformation contour plots

It can be observed in the figure that the maximum, localized in-plane (vertical) and out-of-plane deformation of the module was approximately 0.009 in. and 0.060 in. respectively during the impact event (at maximum crush, t = 0.009 s) and subsequent rebound, t = 0.022 s. Note the localized “hot spots” are more than likely related to surface artifacts on the module (i.e. fasteners and standoffs) and/or shadows from the drop trolley and equipment, resulting in correlation issues. Next, the time-history of the average displacement, as measured across the entire surface of the module, is shown in Figure 32.

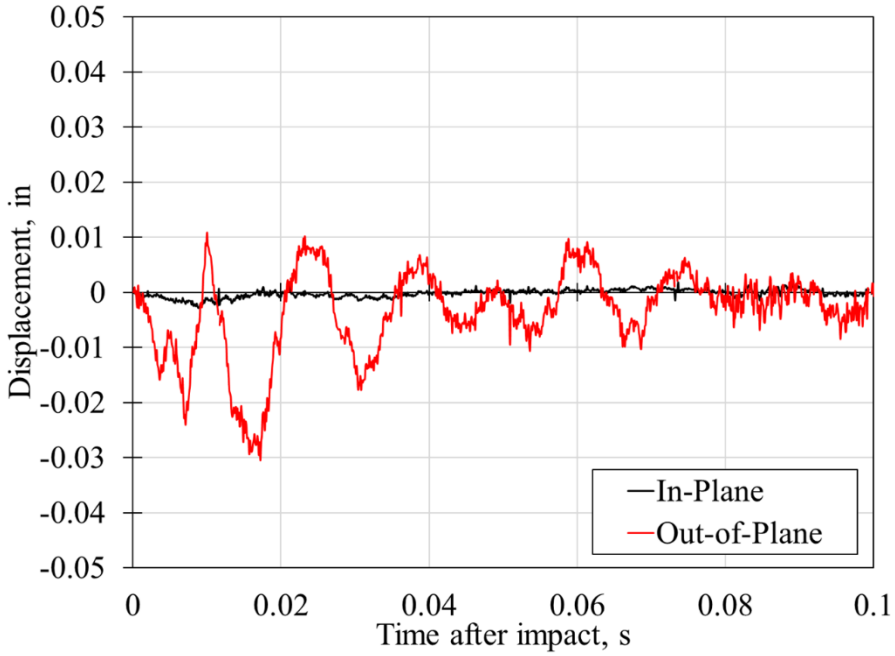

Figure 32. Sideways higher loading condition in-plane and out-of-plane displacement time-history plots

The average in-plane (vertical) deformation was approximately ± 0.003 in., while the average out-of-plane deformation was approximately ± 0.020 in. The axial (vertical) strain of the module, measured using a virtual extensometer across the left edge, center and right edge of the module, is shown in Figure 33. The overall strain response of the module was identical across the surface and ranged between approximately ± 1000 με.

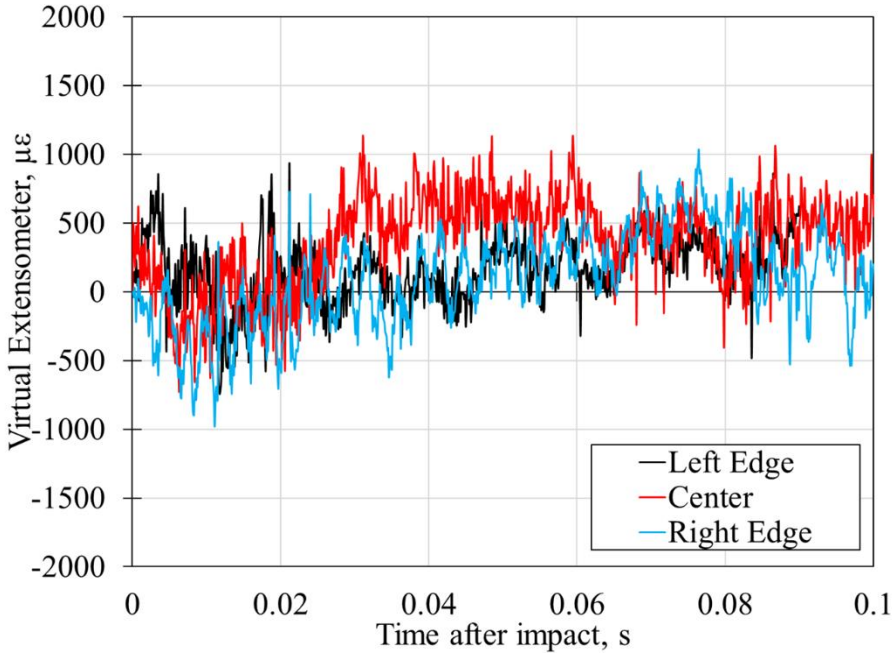

Figure 33. Sideways higher loading condition virtual extensometer time-history plots

Following the test, the post-test passive monitoring was completed, and the post-test forensics inspections occurred. As with the other two tests, the forensics inspections occurred on July 29, 2024, at the EPS

hangar. The inspections began with the Enclosure Assembly. There were several items to note from the Enclosure Assembly. Several of the screws on the enclosure endcap had come loose and did not fasten the endcaps to the Cell Assembly. In addition to the endcap screws, some of the enclosure standoff screws exhibited some deformation. After the Enclosure Assembly was removed, the Containment Assembly was revealed. The end view of the module is shown in Figure 34, with the Cell Assembly shown on the forward face. The Enclosure Assembly is still wrapped around the other faces of the module.

Figure 34. Sideways higher loading condition Containment Assembly

The major item noticed during the inspections of the Containment Assembly was the orientation shift in the standoffs toward the impact side. This deformation was common for the Phase 1 tests but was not yet observed in the Phase 2 testing. This result suggested the impact load was at levels causing the internal components to shift relative to the Enclosure Assembly. At the Cell Assembly level, the standoff holders deformed and actual began to deform the cells on the impact side. This result is shown in Figure 35, which depicts multiple views of the cells themselves.

Figure 35. Sideways higher loading condition cells – end view (left) and side view (right)

The standoff holder motion can be noted by the circular points of deformation in the cell shown in the left image of Figure 35. This type of deformation was also produced in the sideways test from Phase 1, albeit to a much more severe level. However, it should be noted that at this level tested, this type of deformation began to occur. The other main identifiable feature from the inspections of the cells was the deformation due to swelling in the middle cells. This phenomenon is shown in the right of Figure 35, in which the pouch cells are fanning out due to gaps in the middle. In addition to the swelling deformation, there was the presence of electrolyte smell.

The rubric results were compiled and showed that this module had the most amount of damage for the three tests conducted. At the assembly level, the Enclosure Assembly scored "High" values for all three, while at the cell level, damage was observed for several of the categories. There was one cell punctured, which was on the impact side of the module, and 9 of the cells exhibited convex shape deformation due to pouch swelling post-test. There was busbar deformation but no measured electrical shorts, and there was a light presence of electrolyte smell. The Assembly Level total score was 18 while the Cell Damage score was 56, giving a total of 74, which was the highest score, by a significant margin, from the three tests.

Summary

A series of three tests was conducted on ESS modules to generate data on module performance when subjected to attenuated loading conditions meant to better represent an aircraft installed condition. The tests were designed using results obtained from Phase 1, and tailored toward addressing whether improvements in response were able to be identified by examining deformation, damage levels, and rubric scores and making comparisons to Phase 1 data. The test matrix ultimately utilized the two highest scored orientations from Phase 1 and subjecting them to acceleration levels at either 80 g or 220 g.

The first two tests were conducted with modules in the upside down and sideways orientations subjected to a nominal 80-g input acceleration. The desired input levels closely matched the actual input levels for both tests providing a direct comparison between each of the tests. In the Upside Down test, there was no noticeable damage in the Enclosure or Cell Assemblies, with only a slight amount of damage noted in the Containment Assembly due to the fastener orientation change. There did not appear to be any damage in

the cells themselves. In the Sideways test, there was no noticeable damage, and this test received the lowest rubric score from the entirety of Phase 1 and Phase 2 tests.

The third test represented a retest of the sideways module at a higher, 220-g loading condition. In this test, there were signs of damage onset, with each of the three assemblies receiving a "high" score due to endcap protrusion, standoff orientation shift and some deformation. At the cell level, there were indentations and deformations in several of the cells, along with a slight presence of electrolyte. This orientation registered the highest rubric score for the Phase 2 testing.

Discussion

The Phase 2 testing provided several additional data points for which to evaluate the modules and discuss findings. These findings were based both on an examination of only the Phase 2 results, but also making several comparisons between Phase 1 and Phase 2 results. Unlike Phase 1, the Phase 2 results included attenuation in the acceleration levels that were meant to simulate an aircraft installed condition. While this did not completely replicate an actual installed condition, the attenuation into the modules was meant to simulate a generic airframe impact response and was based on as-tested values.

The significantly lower module scores for the 80-g loading levels were correlated little-to-no deformation behavior in the two orientations. Both rubric scores were low – Upside Down at 8 and Sideways at 6, with the Upside Down test article having a higher score due to the orientation change of the standoffs, which was not observed in the Sideways test article. This result suggests the ESS module in its upside down orientation is slightly more suspectable to damage from 80-g impact acceleration than in the sideways configuration. The cell level data were unaffected by orientation change.

When comparing Phase 2 data to Phase 1 data, there are several items to note. In all, when examining only the Phase 2 results, each of the module tests produced rubric scores far below the scores obtained from Phase 1, with only the 220-g sideways test having scores approaching Phase 1 scores. Next, when examining the Upside Down test data, the addition of the attenuation system significantly reduced the amount of damage seen in the enclosures and the cells. Images of the modules in Phase 1 and Phase 2 are shown in Figure 36.

Figure 36. Upside Down test results. Phase 2 80 g (left) and Phase 1 743 g (right)

When comparing the module deformation between the Phase 1 and Phase 2 Upside Down test results, the damage that has developed on the impact facing side of the cells and busbars (at the top in the figure) from Phase 1 is reduced to non-observable levels in the Phase 2 results. There are noticeable amounts of crushing

in the top facing tabs in Phase 1, which has caused the busbars to significantly deform around the tab pattern, whereas in Phase 2, the tabs are still aligned straight up, and the busbars are level. Additional deformation observed away from the impact surface in the cells was also reduced to non-observable levels in the Phase 2 results.

The results from the three tests conducted for Phase 1 and Phase 2, and the higher loading condition from Phase 2 provided additional data for which to compare in the sideways orientation. Images from the module's impact side are shown in Figure 37.

Figure 37. Sideways cell results. Phase 2 80 g (left), Phase 2 220 g (middle), Phase 1 (right)

The sideways orientation tests conducted between Phase 1 and Phase 2 provided valuable insight into how the progressive damage could occur at increasing acceleration levels. The 80-g test results show little to no deformation, which is reflected in the low rubric score. At the 220-g input acceleration level, the module began to show signs of damage and the rubric score increased to levels approaching the lowest levels in Phase 1. The sideways test from Phase 1 provided the highest rubric score out of all tests conducted and showed significant amounts of damage in the cells. Thus, a significant takeaway is the amount of damage developed in the modules was largely dependent on input loading. Furthermore, by attenuating the input loading to reduce maximum acceleration levels, the amount of damage present in the modules and scored in the rubric could be greatly reduced. This result was important because it suggests that accelerations levels within the aircraft will have effects on the resultant response from the ESS modules, and knowing aircraft level accelerations will be able to help guide installation of the ESS within the aircraft itself.

Knowing all of the above, there is a tendency to use the results to generate discussions on expected hazard development such as electrical shorting or TR. However, as previously discussed in the Phase 1 reports, the effect of thermal runaway cannot be directly quantified and correlated to damage seen in the modules due to a variety of factors not tested during the test campaigns. These factors, such as the ZSOC nature of the modules, the lack of details for an actual installed condition, and the lack of other preventative measures in place greatly affect the probability of these types of threats on an actual aircraft installation. Thus, commentary will not be presented other than the discussions on the rubric scores, which is a measurement of damage severity between similar modules under the various tested conditions.

Even with the lack of hazard commentary, the test data did provide additional insight into the nature of damage within the modules with respect to the loading condition. Additional considerations must be given to aircraft specific installations, which include taking into account the surrounding structure of the installed location and the connections, along with other safety improving features such as onboard monitoring capabilities that would be present. While these were not included in Phase 2 testing, NASA is currently

intending on conducting a Phase 3 test in late 2025, which will attempt to address some of these still outstanding items. It is expected that Phase 3 will include several charged modules which will represent a small pack in two orientations with full connections and additional onboard monitoring equipment. While not finalized at the time of writing, the input pulse will be an attenuated pulse similar to Phase 2, however the test will be vehicle agnostic so specific surrounding structure will be absent. Similar measurements are intended to be acquired from the test and presented in future reports.

It is important to note that the test series is utilizing one model ESS module in a single architecture from one OEM, and data presented represents a small piece of a much larger picture. Additional testing spanning various other aspects of ESS design space should be considered to supplement the data provided. Ultimately, the data is intended to generate discussion in the community such that informed decisions can be made with regard to ESS regulation development. In that end, these (and other) tests are important to allow this burgeoning industry to thrive.

Acknowledgements

The authors would like to thank Rob Huculak and his test team at NIAR for conducting the three drop tests. In addition, the authors would like to thank Joseph James, Spencer Wright and Derek Larsen at Electric Power Systems for the support and guidance on the ESS module technical data and for assisting in post-test forensics.

References

1. Federal Register. “Airworthiness Criteria: Special Class Airworthiness Criteria for the Joby Aero, Inc. Model JAS4–1 Powered-Lift.” Volume 89, No. 47. Pages 17230-17264. March 8, 2024.

2. Federal Register. “Airworthiness Criteria: Special Class Airworthiness Criteria for the Archer Aviation Inc. Model M001 Powered-Lift.” Volume 89. No. 102. Pages 45944-45977. May 24, 2024.

3. EASA. “Small Category VCA revision 0.” October 2024.

4. EASA. “Fuel System Crash Resistance.” CS 27.952. CS 27 Amendment 10. February 2023.

5. Littell, J.D. et al. “Dynamic Drop Testing of eVTOL Energy Storage Systems Part 1: Drop Test Data Summary.” Proceedings from Vertical Flight Society’s 81st Annual Forum & Technology Display, May 20-22, 2025, Virginia Beach, Virginia.

6. Littell, J.D. et al. “Dynamic Drop Testing of eVTOL Energy Storage Systems Part 2: Deformation and Post-Test Forensics Results.” Proceedings from Vertical Flight Society’s 81st Annual Forum & Technology Display, May 20-22, 2025, Virginia Beach, Virginia.

7. Jackson, K.E. et al. “A History of Full-Scale Aircraft and Rotorcraft crash Testing and Simulation at NASA Langley Research Center.” 4th Triennial International Aircraft and Cabin Safety Research Conference. November 15-18 2004. Lisbon Portugal.

8. Littell, J.D. “A Comparative Analysis of Two Full-Scale MD-500 Helicopter Crash Tests.” Proceedings from the SEM Annual Conference and Exposition on Experimental and Applied Mechanics, June 13-15, 2011. Uncasville, CT.

9. Littell, J.D. and Putnam J.B. “A Summary of Test Results from a NASA Lift + Cruise eVTOL Crash Test.” Proceedings from the Vertical Flight Society’s 70th Annual Form. West Palm Beach, FL. May 16-18, 2023.

10. Federal Aviation Administration. “Technical Standard Order: Rechargeable Lithium Batteries and Battery Systems.” TSR-C179b. March 23, 2018.

11. United Nations. “Manual of Tests and Criteria, Seventh Revised Edition.” ST/SG/AC.10/11/Rev 7. 2019.

12. Littell, J.D. et al. “Dynamic Testing of eVTOL Energy Storage Systems: Literature Review and Path Forward.” NASA TM 20220015117. January 2023.

13. NIAR-WSU. “NIAR conducts 50-ft eVTOL battery drop test per 14 CFR § 27.952.” December 2, 2022. https://www.wichita.edu/industry_and_defense/NIAR/MediaCenter/2022-12-22.php. Accessed May 5, 2025.